HHS Public Access

Author manuscript

J Bioenerg Biomembr. Author manuscript; available in PMC 2019 September 11.

Published in final edited form as:

J Bioenerg Biomembr. 2016 June ; 48(3): 211–225. doi:10.1007/s10863-016-9664-x.

The non-apoptotic action of Bcl-x_L: regulating Ca^{2+} signaling and bioenergetics at the ER-mitochondrion interface

Abasha Williams[1,2,3], **Teruo Hayashi**[1,4], **Daniel Wolozny**[2], **Bojiao Yin**[2], **Tzu-Chieh Su**[1], **Michael J. Betenbaugh**[2], **Tsung-Ping Su**[1]

[1]Cellular Pathobiology Section, IRP, NIDA, NIH, DHHS, 333 Cassell Drive, Baltimore, MD 21224, USA

[2]Department of Chemical and Biomolecular Engineering, Johns Hopkins University, 3400 North Charles Street, Baltimore, MD 21218, USA

[3]Present address: Division of Biotechnology Review and Research II, FDA/CDER/OPS/OBP, 10903 New Hampshire Ave, Silver Spring, MD 20993, USA

[4]Present address: Seiwakai Nishikawa Hospital, 293-2 Minato-Machi, Hamada, Shimane 697-0052, Japan

Abstract

Bcl-2 family proteins are known to competitively regulate Ca^{2+}; however, the specific inter-organelle signaling pathways and related cellular functions are not fully elucidated. In this study, a portion of Bcl-x_L was detected at the ER-mitochondrion interface or MAM (mitochondria-associated ER membrane) in association with type 3 inositol 1,4,5-tris-phosphate receptors (IP_3R3); an association facilitated by the BH4 and transmembrane domains of Bcl-x_L. Moreover, increasing Bcl-x_L expression enhanced transient mitochondrial Ca^{2+} levels upon ER Ca^{2+} depletion induced by short-term, non-apoptotic incubation with thapsigargin (Tg), while concomitantly reducing cytosolic Ca^{2+} release. These mitochondrial changes appear to be IP_3R3-dependent and resulted in decreased NAD/NADH ratios and higher electron transport chain oxidase activity. Interestingly, extended Tg exposure stimulated ER stress, but not apoptosis, and further enhanced TCA cycling. Indeed, confocal analysis indicated that Bcl-x_L translocated to the MAM and increased its interaction with IP_3R3 following extended Tg treatment. Thus, the MAM is a critical cell-signaling junction whereby Bcl-x_L dynamically interacts with IP_3R3 to coordinate mitochondrial Ca^{2+} transfer and alters cellular metabolism in order to increase the cells' bioenergetic capacity, particularly during periods of stress.

Keywords

Bcl-x_L; Bioenergetics; Calicum signaling; Mitochondria; ER; MAM; IP_3R3

Michael J. Betenbaugh, beten@jhu.edu, Tsung-Ping Su, tsu@intra.nida.nih.gov.

Conflict of interest The authors declare that they have no conflict of interest.

Electronic supplementary material The online version of this article (doi:10.1007/s10863-016-9664-x) contains supplementary material, which is available to authorized users.

Introduction

The endoplasmic reticulum (ER) is the main Ca^{2+} storage facility within cells. ER luminal Ca^{2+} homeostasis and Ca^{2+} signaling are partially maintained and controlled by Ca^{2+} release via three isoforms of inositol 1,4,5-trisphosphate receptors (IP_3Rs; Boehning et al. 2003). In Chinese hamster ovary (CHO) cells, type 3 IP_3R (IP_3R3) resides at the direct ER-mitochondrion contact termed MAM (mitochondria-associated ER membrane) and specifically assist in mitochondrial Ca^{2+} transfer (Mendes et al. 2005). In fact, tethering proteins, such as mitofusin 2 (Mfn2), maintain a distance between the ER and the outer mitochondrial membrane (OMM) of 10–25 nm (Csordás et al. 2006; Hayashi et al. 2009). Thus, IP_3R associate with VDAC on the OMM, through glucose-regulated protein 75, to ensure a large localized increase in Ca^{2+} concentration is obtainable to stimulate mitochondrial Ca^{2+} uptake (Szabadkai et al. 2006). In addition, the sigma-1 receptor (Sig-1R), in conjunction with binding immunoglobulin protein (BiP), forms a complex that stabilizes IP_3R3s at the MAM to prevent degradation and prolong transient Ca^{2+} signals (Hayashi and Su 2007; Su 1982; Snyder and Largent 1989; Largent et al. 1984). This direct mitochondrial Ca^{2+} transfer plays a critical role in the activation of bioenergetics (Cárdenas et al. 2010; Rizzuto et al. 2012; Hammerman et al. 2004). In fact, Ca^{2+} regulates mitochondrial ATP production by targeting Ca^{2+}−dependent enzymes of the TCA cycle (pyruvate, isocitrate, and α-ketoglutarate dehydrogenases) and the electron transport chain as well as ATP synthase and the ATP translocator (Ezawa and Ogata 1979; Bender and Kadenbach 2000; Kirichenko et al. 1998; Hubbard and McHugh 1996; Das 2003; Beis and Newsholme 1976; Jouaville et al. 1999; Wan et al. 1989).

Prolonged Ca^{2+} signals or mitochondrial Ca^{2+} overload disable energetic pathways leading to apoptosis (Pinton et al. 2002). Several members of the Bcl-2 family, known regulators of apoptosis, have also emerged as competitive regulators of intracellular Ca^{2+} at the ER (Lewis et al. 2014). This includes anti-apoptotic Bcl-2 and Bcl-x_L. Both of which bind all three isoforms of IP_3R (Eckenrode et al. 2010) and are known to alter transient Ca^{2+} signals into the cytosol (Eno et al. 2012; Rong et al. 2008; White et al. 2005). It has also been postulated that Bcl-x_L regulation of IP R-mediated Ca^{2+} signals aid in increasing NADPH levels (White et al. 2005). However, direct mitochondrial Ca^{2+} measurements have not been examined. Thus, Bcl-2 family protein involvement in direct ER to mitochondrial Ca^{2+} signaling is unknown. Therefore, we explore the localization and role of Bcl-x_L in the regulation of IP_3R3-mediated mitochondrial Ca^{2+} signaling and bioenergetics as well as its dynamics in CHO cells following stimulus of ER stress.

Herein, Bcl-x_L is shown to reside partially at the MAM, where its BH4 domain is important for IP_3R3 binding. This interaction facilitates the redistribution of Ca^{2+} from the ER to the mitochondria to promote TCA cycle activity, while lowering the transfer of Ca^{2+} into the cytosol. Furthermore, we found that Bcl-x_L translocates to the MAM during ER stress in order to increase interaction with IP_3R3 enriched at the MAM. Thus, Bcl-x_L might exist at the MAM to play an integrating role in bioenergetics and cellular survival by regulating direct mitochondrial Ca^{2+} transients from the ER.

Results

Bcl-x_L resides at mitochondria-associated ER membrane (MAM).

To explore the localization of Bcl-x_L, we fractionated CHOK1 and CHO-Bcl-x_L (CHO-K1 cells stably overexpressing Bcl-x_L) cells into its subcellular compartments (Fig. 1a). Analysis of fractions indicated that endogenous Bcl-x_L was predominately a mitochondrial protein (51 ± 1 %); however, a smaller but distinct amount (12.1 ± 0.8 %) resides in MAM-enriched fractions. The remaining cellular Bcl-x_L was found in whole cell/nuclear (P1), microsomal (P3; vesicle-like artifacts that form from ER fragments), and cytosolic (Cyto) fractions. Overexpressing Bcl-x_L resulted in an overall increase in Bcl-x_L protein (Fig. 1b), although similar percentages of Bcl-xL were observed in most cellular compartments following fractionation (Fig. 1a and Supplemental Figure S1A). An increase in Bcl-x_L detected in the cytosolic fraction was observed, and may be attributed to the abundance of heterologous Bcl-x_L in the overexpressed system. Detection of known nuclear (nucleoporin 62; NP62), mitochondrial (cytochrome c), ER (endoplasmic reticulum resident protein 75; ERp57), MAM (IP_3R3 and Sig-1R), and cytosolic (GAPDH) proteins were used to validate the purity of individual fractions.

Cells were additionally exposed to an alkali treatment (100 mM $NaCO_3$ for 30 min) to determine whether Bcl-x_L binds integrally with cellular membranes (Fig. 1c). Prior to treatment, Bcl-x_L was observed to reside mostly in crude mitochondria fractions (containing MAM). However, after the addition of $NaCO_3$, a majority of endogenous and overexpressing Bcl-x_L was observed in the cytosolic fraction. IP_3R3, a known integral membrane-bound protein used for comparison, resided in membrane fractions before and after alkali treatment. Thus, Bcl-x_L was loosely attached to cellular membranes, which could explain, at least in part, how Bcl-x_L was found in multiple compartments including the mitochondria, MAM, and cytosol.

Bcl-x_L interacts with IP_3Rs and enhances direct mitochondrial Ca^{2+} signaling at the MAM

Given our data indicating Bcl-x_L partially localizes at the MAM (Fig. 1a) and that IP_3R3 is highly enriched at the MAM, we investigated the interaction of Bcl-x_L with IP_3R3 in more detail. IP_3R3 was observed to co-precipitate with Bcl-x_L in CHO-Bcl-x_L cells transiently transfected with IP_3R3 (Fig. 2a). In addition, the binding of Bcl-x_L with endogenous IP_3R3 was investigated by nickel pull-down in CHO-K1 cells transiently expressing full-length, BH4-truncated (ΔBH4), or transmembrane (TM) domain-truncated (ΔTM) polyhistidine (His)-tagged Bcl-x_L constructs (Fig. 2b). We confirm the interaction of full-length Bcl-x_L with endogenous IP_3R3 and normalize this IP_3R3/Bcl-x_L interaction to 100 % (Fig. 2c). In comparison, IP_3R3 binding with Bcl-x_L ΔBH4 (Bcl-x_L lacking the BH4 binding domain giving it its anti-apoptotic activity) was reduced by more than half (44 ± 8 %), and an even greater reduction in IP_3R3 interaction was detected when the TM domain of Bcl-x_L was removed causing Bcl-x_L to become cytosolic, although all of its binding regions remain intact—10± 5 % for Bcl-x_L-ΔTM (Zheng et al. 2008). Thus, the localization of Bcl-x_L to cellular membranes, including the mitochondria and the MAM, and its BH4 binding domain appear to play a role in IP3R3 interaction.

Since IP_3R3 regulates mitochondrial Ca^{2+} signaling at the MAM (Mendes et al. 2005; Blackshaw et al. 2000; Marchi et al. 2012; Bononi et al. 2013), a potential non-apoptotic functional role for Bcl-x_L was explored. We treated cells with 500 nM thapsigargin (Tg) to induce depletion of ER Ca^{2+}. It is important to note that apoptosis is not induced during the time periods considered in this study. In fact, apoptosis was not significantly activated in either cell line following 3 h Tg treatment as indicated by Annexin V positive cells (Fig. 3a), when compared to known apoptosis-inducing compounds staurosporine and camptothecin (Zhang et al. 1998; Gülçe Iz et al. 2012; Hinz et al. 2003). We also evaluated Annexin V positive cells following 12 h Tg treatment, and noted a slight but significant increase in CHO-K1 cells (Fig. 3a). Additionally, there was not a significant increase in caspase 3/7 activity after 3 or 12 h Tg treatment in either cell line (Fig. 3b and Supplemental Figure S2). We monitored intracellular Ca^{2+} after Tg-induced ER Ca^{2+} depletion in co-cultured control and Bcl-x_L overexpressing cells to allow for comparisons under the same microscopy field. HcRed-labeled cell lines (CHO-HcRed and CHO-HcRed-Bcl-x_L) were used to monitor ER and cytosolic Ca^{2+} measurements using D1ER camleon (a yellow fluorescent protein to cyan fluorescent protein FRET-based Ca^{2+} probe targeted to the ER) or Fluo-4 AM (a green-fluorescent Ca^{2+} indicator), respectively. Whereas, YFP-labeled cell lines (CHO-YFP and CHO- YFP-Bcl-x_L) were used to monitor mitochondrial Ca^{2+} using X-Rhod-5f AM, a red-fluorescent Ca^{2+} indicator. Bcl-x_L expression in these cell lines is provided in Supplemental Figure S1B. No significant difference in the rate of intra-ER Ca^{2+} depletion was detected in Bcl-x_L overexpressing cells compared to control cells (Fig. 4a). However, Bcl-x_L overexpressing cells showed a reduced flux of Ca^{2+} transients into the cytosol (Fig. 4b), and interestingly, an increase in transient mitochondrial Ca^{2+} influx (Fig. 4c and Supplemental Figure S3A) following Tg stimulation.

Furthermore, we monitored cytosolic and mitochondrial Ca^{2+} in CHO-Bcl-x_L cells following a reduction in IP_3R3 levels in CHO-Bcl-x_L cells using siRNA (Fig. 4d). Null cells (cells not treated with siRNA) were co-cultured with cells transfected with either control (CNT) siRNA or siRNA targeted to IP_3R3, and either YFP or HcRed vector (depending on the fluorescence of the Ca^{2+} indicator used) in order to distinguish between null and siRNA treated cells. While IP_3R3 knockdown had no significant effect on Ca^{2+} transients into the cytosol (Fig. 4e), an abrogation of mitochondrial Ca^{2+} transfer was observed when compared to null and CNT siRNA treated cells (Fig. 4f). An observed change in the initial slope of mitochondrial Ca^{2+} transients following CNT siRNA treatment is noted (Fig. 4f); however, nonspecific effects are common (Scacheri et al. 2004) and we expected to see some changes compared to cells without any siRNA. Similar results were also seen in CHO-K1 cells following IP_3R3 knockdown (Supplemental Figure S3B–C). In contrast, we did not observe any significant differences in mitochondrial Ca^{2+} transients following knockdown of IP_3R1 and IP_3R2 (data not shown). These findings suggest that increased levels of Bcl-x_L, particularly at the MAM, serve to aid in the distribution of ER Ca^{2+} transients into the mitochondria.

Bcl-x_L expression enhances Ca^{2+}− dependent bioenergetics

Metabolic phenotyping was performed in order to examine whether there are any bioenergetic implications of Ca^{2+} redistribution due to Bcl-x_L expression. Microarray plates

were used to measure the metabolic consumption of nine metabolites that feed into the TCA cycle (D-mannose, D,L-lactate, pyruvate, α-keto-glutarate, succinamic acid, succinate, mono-methyl succinate, adenosine, and inosine) as a function of NADH flux (Supplemental Figure S4). Wells containing glucose served as a positive control, while tricarballylic acid wells functioned as a negative control by hindering the conversion of citrate in the TCA cycle (Russell and Forsberg 1986). Utilization rates of substrates were normalized to the slope of glucose consumption, and overall, Bcl-x_L overexpressing cells tended to consume these metabolic substrates at a higher rate than controls (Fig. 5a). Additionally, endogenous lactate accumulation was measured on a per cell basis, and CHO-Bcl-x_L accumulated lower levels of lactate compared to controls (Fig. 5b), suggesting pyruvate is shuttled into the TCA cycle more efficiently in these cells.

NAD/NADH ratio was also investigated since NAD is reduced to NADH in the TCA cycle. Compared to control cells, Bcl-x_L overexpressing cells had higher levels of NADH relative to NAD, thus the NAD/NADH ratio was lower (Fig. 5c), which indicate Bcl-x_L overexpressing cells have a more active TCA cycle compared to controls. Cells were also subjected to short treatments with Tg (15 or 30 min) to induce increases in mitochondrial Ca^{2+} as previously observed in Fig. 3c. Under these conditions, NAD/NADH ratios decreased in both cell lines, although ratios still tend to remain lower in Bcl-x_L over-expressing cells (Fig. 5c). In contrast, higher NAD/NADH ratios were noted in both cell lines after IP_3R3 was knocked down and remained high following 30 min treatment with Tg (although a slight drop was noted in the CHO-Bcl-x_L cells which can be attributed to the remaining IP_3R3 following knockdown), while CNT siRNA had no significant affect in comparison to controls (Fig. 5d).

NADH generated from the TCA cycle is subsequently fed into the electron transport chain (ETC.) where it is oxidized by enzymes known as oxidoreductases. Therefore, we used a chemiluminescence assay to monitor the activity of mitochondrial oxidoreductases of the ETC. (ETC oxidase activity) in cells stimulated with NADH (Michel et al. 1998; Lu et al. 2007). Interestingly, Bcl-x_L overexpressing cells were observed to have higher ETC oxidase activity compared to control cells following stimulation with NADH (Fig. 5e), and similar results were seen using YFP- and HcRed-tagged Bcl-x_L and their control counterparts (Supplemental Figure S5). Additionally, the inclusion of chemicals that change intracellular Ca^{2+} availability were shown to alter ETC oxidase activity (Fig. 5e), especially for Bcl-x_L overexpressing cells. For example, 30 min incubation with Tg increased ETC oxidase activity. Whereas, treating cells for 30 min with BAPTA-AM, a Ca^{2+} chelator that reduces intracellular Ca^{2+} concentration, hindered ETC oxidase activity even after an additional treatment with Tg. Thus, ETC activity appears to be dependent on Bcl-x_L levels and Ca^{2+} availability, perhaps as a result of more rapid TCA cycling and NADH turnover. Taken together, the data indicates that Ca^{2+} redistribution as a result of Bcl-x_L overexpression alters mitochondrial metabolism and NADH generation.

Bcl-x_L translocates to the MAM and increases bioenergetic capacity following thapsigargin-induced ER stress

We were also interested in determining how Bcl-x_L expression affects bioenergetics under stress conditions. While we have shown that 3 h treatment with Tg does not stimulate apoptosis (Fig. 3), prolonged Tg treatment has previously been shown to cause ER stress in CHO cells (DuRose et al. 2006), so we investigated whether ER stress is activated in our cells after extended periods of Tg insult. Following a 1 or 3 h incubation with Tg, we did not see any changes in endogenous or overexpressed Bcl-x_L expression levels (Fig. 6a). However, we did observe an upregulation of phosphorylated PERK (pPERK), an ER resident protein that becomes activated during ER stress (Mori et al. 2013), in both cell lines after 1 or 3 Tg treatment (Fig. 6b). Although, significantly more upregulation of pPERK was observed in CHO-K1 cells in comparison to pPERK upregulation in Bcl-x_L overexpressing cells.

Since extended Tg treatment induces ER stress in our cells, we next examined for potential bioenergetic implications. NAD/NADH ratios were reduced in both control and Bcl-x_L overexpressing cells after 1 h Tg treatment, and even more so after 3 h incubation (Fig. 6c). Furthermore, ETC oxidase activity increased to a greater extent following NADH stimulation in both cell lines after 3 h Tg treatment when compared to the increase in activity without any Tg (Fig. 6d). Pre-treating cells with BAPTA again diminished increases in ETC oxidase activity due to Tg stimulation (Fig. 6d). Overall,TCA cycle activity again remained higher in Bcl-x_L overexpressing cells. Given this information and that we previously show that MAM-associated Bcl-x_L aids in stimulating TCA cycle activity, we investigated whether Bcl-x_L localization at the MAM was altered before and after prolonged Tg treatment.

Endogenous Bcl-x_L levels did not provide sufficient signal to quantify Bcl-x_L localization by microscopy. Thus, immunostained CHO-Bcl-x_L cells transiently transfected with GFP-mito, a mitochondrial marker, were examined by 3D confocal microscopy (Fig. 7a). After imaging 50 individual cells and isolating 300 individual mitochondria, we found that mitochondria-associated Bcl-x_L existed predominately in clustered form on or around mitochondria. As such, Bcl-x_L was categorized into three distribution patterns based on its relation to mitochondria—Type 1: Clustered on mitochondria, Type 2: Clustered next to mitochondria, and Type 3: Evenly distributed, or not clustered, on mitochondria (Fig. 7b). The characterization of Bcl-x_L into these distribution patterns was determined by first distinguishing between Bcl-x_L that was either in clustered form or non-clustered form. Those that were in non-clustered form were characterized together as Type 3, and later found to have >80 % of Bcl-x_L colocalized with mitochondria. Next, Bcl-x_L in clustered form was additionally observed to either overlap, or sit adjacent to the mitochondria marker. Therefore, we further distinguished clustered Bcl-x_L based on its colocalization with mitochondria. Those that had ≥50 % of Bcl-x_L colocalized with mitochondria were characterized as Type 1, and those that had <50 % of Bcl-x_L colocalized with mitochondria were characterized as Type 2 (data not shown).

We then grouped individual mitochondria based on the aforementioned distribution patterns of associated Bcl-x_L (Fig. 7c). Mitochondria with exclusively Type 1 Bcl-x_L were the most

prominent (43 ± 4 %), while 23± 4 % of mitochondria exhibited Bcl-x_L in a Type 2 pattern and 1.4 ± 0.8 % of mitochondria were observed with Type 3 Bcl-x_L. The remaining ~30 % of mitochondria were observed to have more than one type of cluster or have a combination of evenly distributed and clustered Bcl-x_L forms. Similar Bcl-x_L distribution patterns were observed when alternatively using endogenous Tomm20 as a mitochondrial marker, and with CHO-K1 cells stably overexpressing varying levels of YFP- or HcRed-tagged Bcl-x_L (Supplemental Figure S6A–C). Additionally, we observed that mitochondrial staining was similar in CHO-K1 and CHO cells expressing various levels of Bcl-x_L (Supplemental Figure S6D).

Clustered Type 1 and Type 2 Bcl-x_L were examined further to determine if they might associate with the MAM. Confocal microscopic examination was repeated as previously described with the addition of a MAM marker protein, IP_3R3, and Mfn2, a MAM-mitochondria tethering protein (Supplemental Figure S7A). In Fig. 7d, Type 1 Bcl-x_L was observed to sit adjacent to the MAM and a fraction even colocalized with IP_3R3 (18 ± 2 %) and Mfn2 (17 ± 3 %). Type 2 Bcl-x_L also sat adjacent to MAM markers (Fig. 7d). However, we detected greater colocalization with IP_3R3 (38 ± 5 %), and interestingly 76± 4 % of the Type 2 Bcl-x_L co-localized with Mfn2. This data indicates that Type 2 Bcl-x_L was clustered alongside mitochondria in the region associated with the MAM, and can be explained in part by our findings in Fig. 1c showing that Bcl-x_L is a peripherally-attached membrane-bound protein. Furthermore, Bcl-x_L colocalization with other ER-resident proteins enriched at the MAM—Sig-1R and BiP—was found to be similar to that of IP_3R3 (Supplemental Figure S7A–B). Thus, a putative schematic representative of Type 1 and Type 2 Bcl-x_L association with mitochondria and MAM markers is illustrated in Fig. 7e. Of note, we did not observe significant co-localization between MAM marker proteins and GFP-mito, with the exception of Mfn2 (Supplemental Figure S7C).

Next, we examined the effect of extended Tg treatment on Bcl-x_L localization. In immunostained CHO-Bcl-x_L cells, the percentage of mitochondria with exclusively Type 1 Bcl- x_L decreased from 43± 4 % to 4 ± 2 % follow 3 h Tg treatment, while there was a corresponding increase in mitochondria with Type 2 MAM-associated Bcl-x_L from 23± 4 % to 59± 5 % (Fig. 8a). Likewise, in living cells, YFP-tagged Bcl-x_L co-localization with mitochondria, labeled with DsRed-mito, decreased from 73± 3 % to 44± 4 % during 3 h incubation with Tg (Fig. 8b). Moreover, results from cell fractionation indicate that Bcl-x_L in MAM-enriched fractions increased following 1 or 3 h Tg treatment (Fig. 8c). Tg-stimulated translocation of Bcl-x_L was also observed to increase total cellular interaction of Bcl-x_L with IP_3R3 as detected by immunoprecipitation (Fig. 8d) and nickel pull-down (Fig. 8e). Taken together, these data indicate that Tg-induced ER stress triggers Bcl-x_L trans-location to the MAM region where it increases its interaction with IP_3R3, known to be enriched at the MAM, in order to alter cellular bioenergetics. Furthermore, we note the same tendency in cells treated with tunicamycin over an extended period of time (Supplemental Figure S2 and S8).

Discussion

Bcl-x_L has previously been determined to reside predominately at the mitochondria at both the inner and outer membranes (Chen et al. 2011; Kaufmann et al. 2003), which correlates with a another study that shows that the X-TMB sequence— the C-terminal transmembrane (TM) domain of Bcl-x_L flanked by two basic regions, namely X and B—is responsible for mitochondrial targeting (Kaufmann et al. 2003). However, Bcl-x_L is also known to be partially present at the ER and within the cytosol (Tagami et al. 2000). Our subcellular fractionation study is in agreement with these previous observations and we find that a majority of peripherally bound Bcl-x_L resides in mitochondria-enriched fractions, and is also present in microsomal (ER) and cytosolic fractions. Interestingly, we also observed for the first time that Bcl-x_L was partially localized in MAM-enriched fractions. This data is consistent with a previous study by our group in which Bcl-2 was observed to reside in part at the MAM (Meunier and Hayashi 2010). However, there has been little investigation to determine if Bcl-2 family members serve a specific role at this cellular location. Thus, in this study we explored the functional implications of Bcl-x_L at the MAM under non-apoptotic conditions.

Bcl-x_L has previously been found to physically interact with all three isoforms of IP_3Rs (White et al. 2005; Eckenrode et al. 2010), and modulate the expression of type 1 and 3 IP_3Rs (Li et al. 2002). We confirmed the interaction of Bcl-x_L with IP_3R3, which is known to be enriched at the MAM, and additionally determined that the BH4 domain of Bcl-x_L may be particularly relevant for IP_3R3 binding. Previous results indicate that the BH4 domain of Bcl-2 is required for interaction with domain 3 of IP_3Rs. However, the BH4 domain of Bcl-x_L was not observed to bind this domain (Monaco et al. 2012; Rong et al. 2009), but full-length Bcl-x_L was found to bind domain 6 of IP_3R (White et al. 2005). Membrane targeting of Bcl-x_L also seems to be crucial for Bcl-x_L interaction with IP_3R3 as indicated by the limited interaction of Bcl-x_L ΔTM with IP_3R3, since Bcl-x_L is cytosolic when lacking its TM domain (Zheng et al. 2008).

Due to its interaction with IP_3R3, a possible functional role for Bcl-x_L in IP_3R3-mediated Ca^{2+} signaling was investigated (Szabadkai et al. 2006). In the current study, there was relatively little difference in the rate of Tg-induced ER Ca^{2+} depletion in CHO-K1 and CHO-Bcl-x_L cells expressing endogenous levels of all isoforms of IP_3R. This is consistent with a previous report showing Bcl-x_L expression had no effect on releasable ER Ca^{2+} stores in CHO cells stably expressing ryanodine receptors, an ER Ca^{2+} release channel (Pan et al. 2000). However, the role of Bcl-x_L in ER luminal Ca^{2+} homeostasis appears to be cell type dependent. For instance, reduced ER luminal Ca^{2+} in DT40 cells expressing Bcl-x_L was attributed to IP_3R3 expression (Li et al. 2007), and a Bcl-x_L variant targeted to the ER was shown to reduce ER Ca^{2+} stores in MEF cells (Eno et al. 2012). Nonetheless, we saw limited increases in cytosolic Ca^{2+} levels in Bcl-x_L over-expressing cells immediately following short-term Tg stimulation that is in agreement with past studies (White et al. 2005; Chen et al. 2004; Distelhorst and Shore 2004). However, mitochondrial Ca^{2+} levels were not previously examined nor were mechanisms for mitochondrial Ca^{2+} entry demonstrated. We measured mitochondrial Ca^{2+} levels directly and found that Bcl-x_L enhances transient increases in mitochondrial Ca^{2+} following stimulation. In fact, mitochondrial Ca^{2+} transport

occurs in parallel with cytosolic Ca^{2+} release. Thus, the differences in the rate of Ca^{2+} increase in the two compartments suggest direct Ca^{2+} transport into the mitochondria is aided by Bcl-x_L. In further support, we report the reduction of mitochondrial Ca^{2+} uptake in cells depleted of IP_3R3, which is consistent with a previous study from our group showing that IP_3R3 knockdown significantly reduced ATP-induced mitochondrial Ca^{2+} transients (Hayashi and Su 2007). Thus, we hypothesize that Bcl-x_L interaction with IP_3R3 at the MAM aids in the facilitation of direct mitochondrial Ca^{2+} transport, although we cannot exclude the possibility of some Bcl-x_L or IP_3R3 interactions playing a role in other cellular compartments.

There are multiple possible mechanisms by which Bcl-x_L may facilitate mitochondrial Ca^{2+} transport. One mass action mechanism may be that interactions between Bcl-x_L and IP_3R3 facilitate a build-up of Ca^{2+} in the region around the MAM, leading to a concentration driven increase in mitochondrial Ca^{2+} transport. Bcl-x_L/IP_3R3 binding may also facilitate a conformational change to increase Ca^{2+} pumping or binding to other partners, such as VDAC, to enhance Ca^{2+} transfer. Additionally, IP_3R3-mediated Ca^{2+} transfer may be supported by Bcl-x_L interaction with VDAC. Indeed, a recent report shows that Bcl-x_L knock-out in MEF cells reduces mitochondrial Ca^{2+} uptake relative to controls, while mitochondria-targeted Bcl-x_L was shown to enhance mitochondrial Ca^{2+} uptake by interacting with VDAC in permeabilized cells (Huang et al. 2013). While these three alternatives are in fact complementary, further investigations will be required to elucidate the specific mechanism(s) by which Bcl-x_L serves to enhance direct mitochondrial Ca^{2+} shuttling. Nonetheless, our current study sheds light on at least one mechanistic pathway for explaining the drop in mitochondrial Ca^{2+} uptake previously observed in MEF cells lacking Bcl-x_L (Huang et al. 2013).

This study additionally provides support to the notion that Bcl-x_L evolved to include multiple intracellular functionalities. We propose that Bcl-x_L plays a critical role in bioenergetics as a result of increases in direct ER to mitochondrial Ca^{2+} transfer. This mitochondrial stimulation is known to increase Ca^{2+}− dependent enzymes of the TCA cycle in order to provide sufficient energy to promote proper cell functioning (Cárdenas et al. 2010; Hammerman et al. 2004; Rizzuto et al. 2012). Indeed, our data show that Bcl-x_L overexpression causes global increases in metabolite consumption, decreases in lactate accumulation, lower NAD/NADH ratios, and higher ETC oxidase activity that suggest Bcl-x_L overexpression alters TCA cycle activity in particular. Other mechanisms, such as an increase in metabolic transporters, may also play a role. Previous studies also support a role for Bcl-2 family proteins in altering cellular metabolism. For example, Bcl-x_L expression was found to increase resting NADPH levels in DT40 cells (White et al. 2005). Bcl-2 increased oxygen consumption and rates of mitochondrial respiration (Chen and Pervaiz 2007, 2010). Furthermore, overexpression of Bcl-2 family proteins in various cell lines reduces lactate accumulation (Dorai et al. 2009; Jeon et al. 2011). A study in CHO-S cells overexpressing Bcl-2Δ showed that reduced lactate was the result of the redirection of pyruvate toward mitochondrial oxidation to stimulate TCA cycle activity (Templeton et al. 2014).

We additionally determined that Bcl-x_L expression affects bioenergetics under stress conditions after a closer inspection of Bcl-x_L localization at the MAM following prolonged Tg treatment. Indeed, we provide evidence of the first case of Bclx_L reorganizing to the MAM during an ER stress event. By confocal microscopy analysis, we observed three distinct distribution patterns of membrane-bound Bcl-x_L in relation to mitochondria: (1) Clustered on mitochondria, (2) Clustered next to mitochondria, and (3) Evenly distributed on mitochondria. Type 2 Bcl-x_L was of particular interest as it was found to associate most significantly with the MAM. Following extended Tg treatment, which induces ER stress but does not stimulate apoptosis, we observed Bcl-x_L translocation from the mitochondria to the MAM and an increase in Bcl-x_L interaction with IP_3R3. Increased Bcl-2 and Bcl-x_L interaction with IP_3R3 has also been observed after apoptosis is induced with tyrosine kinase inhibitors (Zannetti et al. 2008). We postulate that this interaction is localized to the MAM and believe the reason is to drive Ca^{2+} transients into the mitochondria as a way to stimulate TCA cycle activity.

Bcl-x_L regulation of bioenergetic pathways would be particularly important during times of cellular stress. We found that Bcl-x_L expression is able to modulate cellular response to ER stress induced by sustained Tg treatment by increasing the bioenergetic capacity of the cell. We observed significant reduction in the upregulation of ER stress in cells overexpressing Bcl-x_L, as indicated by reduced increases in pPERK (Su et al. 2008). This is accompanied by a further reduction in NAD/NADH ratios and even greater ETC oxidase activity in cells following prolonged Tg insult, and is consistent with previous reports showing an increased metabolic need in cells during times of stress (Duchen 2004; Gautier et al. 2008; Addabbo et al. 2009). In fact, ATP production is necessary for maintaining cell functioning, and a reduction in ATP levels and the ability of cells to handle nutrient stress was observed in *Drosophila* mutants without the Bcl-2 family protein Buffy (Monserrate et al. 2012). The ER, in particular, requires an adequate supply of energy to promote proper protein folding and clearance of misfolded proteins (Berridge 2002; Görlach et al. 2006; Hoseki et al. 2010). Thus, increasing mitochondrial Ca^{2+} transients to promote cellular metabolism can represent a means of trying to fend off insults during the adaptive stress response, whereas cells with impaired ER to mitochondrial Ca^{2+} transport are more susceptible to apoptosis (Jahani-Asl et al. 2007; Brooks et al. 2011). In fact, an increase in the physical connection of the ER and mitochondria was observed during the very early stages of ER stress and was shown to support mitochondrial Ca^{2+} transport (Bravo et al. 2011). These increases in MAM contact sites may be supported by Mfn2 tethering of the MAM and mitochondria. In a recent study, an upregulation of Mfn2 mRNA and protein levels was demonstrated, but no change in the expression of mitochondria shaping proteins was detected, following Tg- or tunicamycin-induced ER stress (Ngoh et al. 2012). These data once again support our observations showing Bcl-x_L translocation from mitochondria to the MAM. Possibly due to an increase in the number of ER-mitochondria contact sites during sustained Tg treatment.

The ability of Bcl-x_L to control mitochondrial Ca^{2+} homeostasis in order to maximize bioenergetics may ultimately be undermined during the initiation of apoptosis. Indeed, proapoptotic proteins Bax/Bak and tBid activated during ER stress (Upton et al. 2008) displace Bcl-2/Bcl-x_L interaction with type 1 IP3R (Oakes et al. 2005; White et al. 2005), while Bax/Bak were additionally shown to increase ER Ca^{2+} leakage (Scorrano et al. 2003;

Oakes et al. 2005). Sustained Ca^{2+} leakage directly into the mitochondria has been linked to the modulation and upregulation of IP_3R3 (Giorgi et al. 2010; Blackshaw et al. 2000; Marchi et al. 2012; Bononi et al. 2013) and MAM integrity (Betz et al. 2013). Ultimately, mitochondrial Ca^{2+} overload will disable metabolic pathways and lead to apoptosis (Pinton et al. 2002). As a result, cyto-chrome c is released into the cytosol where it is then able to bind IP_3Rs to boost apoptotic Ca^{2+} signals (Boehning et al. 2003). Thus, our findings suggest that non-apoptotic Bcl-x_L regulation of mitochondrial Ca^{2+}, particularly at the MAM, is especially complex and multifunctional with a very stringent yet fine control that responds differently to various levels of cellular stress.

Materials and methods

Cell culture and transfection

All cells were grown in Ham's F-12 Nutrient Mixture supplemented with 1 mM L-glutamine and 10 % heat-inactivated fetal bovine serum (Life Technologies). Cells were maintained at 37°C in 5 % CO_2. CHO-pcDNA cells were obtained by stable transfection of parent null vector pcDNA3.1/Neo(+) into CHO-K1 cells; herein CHO-pcDNA cells will be referred to simply as CHO-K1. CHO-Bcl-x_L cells were obtained by stable transfection of the expression vector pBcl- xL-neo as previously described (Chiang and Sisk 2005). Expression vectors for pYFP-Bcl-x_L and pHcRed-Bcl-x_L encoding YFP-Bclx_L or HcRed-Bcl-x_L fusion proteins were created by PCR amplification of YFP and HcRed from pEYFP-C1 or pHcRed-N1 vectors, respectively (Clonetech), and ligation into pBcl-x_L-neo. CHO-YFP and CHO-HcRed cells were obtained by transfecting pEYFP-C1 or pHcRed-N1 into CHO-K1 cells. Human Bcl-x_L ΔBH4 (lacking amino acids 2–24) or Bcl-x_L ΔTM (lacking amino acids 205–233) proteins constructs, kindly provided by J.M. Hardwick (Johns Hopkins University, Baltimore, MD), were PCR amplified and ligated into pcDNA4/HisMax. All plasmids were stably transfected into CHO-K1 cells using PolyJet (SignaGen) or Lipofectamine 2000 (Life Technologies). Selection in the presence of G418 was used to obtain all stable clones. PepMute siRNA transfection reagent (SignaGen Laboratories) was used to transfect cells with inactive (CNT) or active siRNA targeting IP_3R3. Sense sequences for siRNA were previously described (Hayashi and Su 2007).

Subcellular fractionation

MAM was prepared as described previously (Vance 1990). Following homogenization of CHO-K1 or CHO-Bcl-x_L cells grown on 15-cm dishes, the nuclear/whole cell (P1), crude mitochondrial, and microsomal fractions (P3) were prepared by differential centrifugation. Supernatants were collected as the cytosolic fraction. The crude mitochondrial fraction in isolation buffer (250 mM mannitol, 5 mM HEPES, 0.5 mM EGTA, pH 7.4) was subjected to Percoll gradient centrifugation for separation of the MAM from mitochondria. Once all fractions were collected, protein concentration in each sample was assessed using a BCA protein assay kit (ThermoFisher Scienific). Samples were then boiled in 2X sample buffer and equal amounts of total protein from each fraction were analyzed by SDS-PAGE and western blotting.

Pull-down assays

CHO-Bcl-x_L transiently transfected with IP_3R3 were incubated in 1X TN lysis buffer (50 mM Tris–HCl at pH 7.4, 150 mM NaCl, and 1 % Triton X-100, pH 7.4) for 30 min on ice. Cells were harvested in lysis buffer and rotated for 15 min at 4°C. After centrifugation at 12,000× g, the supernatant was pre-cleared with Sepharose protein A beads (GE Healthcare) and incubated overnight with primary anti-IgG or anti-Bcl-x_L antibodies at 4°C. The lysate was then incubated with Sepharose protein A beads for 90 min at 4°C. After washing with lysis buffer, protein concentration was assessed using a BCA protein assay kit. Immunoprecipitants were then boiled in 2X sample buffer, and equal amounts of total protein from each sample was analyzed by SDS- PAGE and western blotting.

CHO-K1 cells transiently transfected with pcDNA4-Bcl-x_L (His-tagged Bcl-x_L) were seeded on 6-well plates until 100 % confluent. Cells were washed twice with PBS and incubated in 1X TN lysis buffer for 30 min on ice. Then cells were harvested and rotated for 15 min at 4°C. After centrifugation at 12,000× g, supernatants were incubated with 30 µl ProBond Ni^{2+} − Chelating Resin (Life Technologies) for 90 min at 4°C. Resin was washed three times with lysis buffer (pH 6). After samples were analyzed for protein concentration (Bradford protein assay; ThermoFisher Scentific), equal amounts of total proteins from each sample were evaluated by SDS-PAGE and western blotting.

Ca^{2+} flux experiments

Control (CHO-YFP or CHO-HcRed) and Bcl-x_L overexpressing (CHO-YFP-Bcl-x_L or CHO-HcRed-Bcl-x_L) cells were co-cultured on coverslips with poly-D-lysine coating. Additionally, null (non-siRNA treated) and siRNA treated (CNT or IP_3R3, and pEYFP-C1 or pHcRed-N1) cells were co-cultured on coverslips with poly-D-lysine coating. ER Ca^{2+} was labeled using a FRET-based sensor D1ER Ca^{2+} cameleon in pcDNA3 (kindly donated by R.Y. Tsien, University of California); characterization of D1ER was reported previously (Palmer et al. 2004). Cells were transfected with D1ER 24 h prior to imaging. YFP and CFP intensities were corrected for background and net FRET (nF) fluorescence was previously defined as follows (Palmer and Tsien 2006; Xia and Liu 2001):

$$nF = I_{FRET} - \left(I_{YFP} \times YFP_{bleed-through}\right) - \left(I_{CFP} \times CFP_{bleed-through}\right)$$

Where I_{FRET}, I_{YFP}, and I_{CFP} are fluorescence intensities under FRET, YFP, and CFP filter sets respectively. Bleed-through constants, $YFP_{bleed\text{-}through}$ and $CFP_{bleed\text{-}through}$, are the percentage of YFP or CFP, respectively, detected under the FRET filter set. Cytosolic and mitochondrial Ca^{2+} was labeled using Fluo-4 AM and X-Rhod-5f AM Ca^{2+} dyes, respectively. Cells were incubated in dye for 20 min followed by washing (15 min) or transfected with GCaMP5 24 h prior to imaging. Ca^{2+} flux as a measure of fluorescence intensity (F) was determined by capturing images every minute for 30 min using a spinning disk confocal system (Ultraview, PerkinElmer) and inverted microscope (Nikon Eclipse TE2000-E), and a 60× (NA 1.4) or 40× (NA 1.3) oil objective, while perfusing with Krebs-HEPES Buffer (KHB) containing 100 mM HEPES, 640 mM NaCl, 12.5 mM KCl, 5 mM Mg Cl_2, 80 mM glucose and 1.5 mM $CaCl_2$, or KHB without Ca^{2+} and 0.5 mM LaCl3.

Metabolic assays

CHO-K1 and CHO-Bcl-x_L cells suspended in IF-M2 media (Biolog) supplemented with 0.3 mM glutamine were seeded (20,000 cells/well) onto Phenotype Microarray PM-M1 plates (Biolog, Hayward, CA) containing 91 carbon-energy sources. Cells were incubated at 37°C and 5 % CO_2 for 2 h until glutamine was depleted; thus the metabolites contained in each well of the PM-M1 plates became the sole nutrient source for the cells. Cells were then incubated for an additional 12 h in an OmniLog automated incubator-reader (Biolog) at 37°C with Redox Dye Mix MB (Biolog), a tetrazolium-based dye. During this incubation period, metabolite utilization was measured as a function of NADH flux, which in return is based on the rate of dye reduction (Berridge et al. 2005). Wells containing glucose served as a positive control, while wells containing tricarballylic acid functioned as a negative control since it hinders the conversion of citrate in the TCA cycle (Russell and Forsberg 1986). Since we were interested in the mitochondrial bioenergetic differences between CHOK1 and CHO-Bcl-x_L, utilization rates of 9 key metabolites known to feed into the TCA cycle were analyzed (see figure legend). Metabolite utilization for all substrates was normalized to the slope of glucose consumption. Lactate was measured from media samples taken from CHO-K1 and CHOBcl-x_L cells seeded in 6-well plates after 48 h. Cells were then washed with PBS and cultured in glucose-free DMEM media (Life Technologies) for 30 min. Media was then supplemented with 6 mM D-glucose. Culture media samples were collected every 30 min and diluted 5 times with 150 mM Tris–HCl (pH 8.8).

Diluted culture media and standards were placed on clear 96-well plates and incubated at room temperature for 20 min. L-lactate was assayed by addition of 100 μl of color reagent per well: 2 mM 2-(p-Iodophenyl)-3-(pnitrophenyl)-5-phenyltetrazolium chloride, 3 mM NAD^+,2 mM ml L-lactate/ml L-lactate dehydrogenase. Absorbance was measured at 550 nm using a Genios plate reader (TECAN).

An NAD/NADH Quantitation Kit (Sigma-Aldrich) was used to measure NAD_{total} (total NADH and NAD) and NADH in CHO-K1 and CHO-Bcl-x_L cell lysates according to the manufacture's instructions. Standards and samples were colorimetrically assayed on clear 96- well plates using a Genios plate reader (TECAN) at 450 nm. A chemiluminescence assay was used to measure electron transport chain oxidoreductase (ETC oxidase) activity in CHO-K1 and CHO-Bcl-x_L cells harvested in PBS. Suspended cells (5–6 × 10^5 cells per well) were placed on white 96-well plates with solution containing PBS and 20 μM lucigenin and luminescence was monitored for 5 min using VICTOR 3 plate reader (PerkinElmer). Following NADH (45 μM) stimulation (Lu et al. 2007; Michel et al. 1998), luminescence was additionally monitored for 60 min.

Cellular stress assays

CHO-K1 and CHO-Bcl-x_L cells were cultured on sterile black 96-well plates and pretreated with 500 nM Tg, 3 μM staurosporine (STA) or 50 μM camptothecin (Camp). Apoptosis was then analyzed using an Annexin V FITC Assay Kit (Cayman Chemical) or a Caspase-Glo Assay Kit (Promega) using either a VICTOR 3 plate reader (PerkinElmer) or a Genios plate reader (TECAN), respectively.

Immunostaining

CHO-Bcl-x_L cells were transiently transfected with GFP-mito (pAcGFP1-mito; Clonetech) or DsRed-mito (pDsRed2-mito; Clonetech) mitochondrial markers and grown on coverslips with poly-D-lysine coating. After fixation with 4 % paraformaldehyde in 0.1 M phosphate buffer, cells were permeabilized with 0.2 % Triton X-100 or 0.1 % NP-40 for 10 min. Cells were then incubated with 10 % nonfat milk to block against non-specific binding of antibodies. Fixed cells were then incubated with monoclonal Tomm20 (translocase of outer mitochondrial membrane 20; Abcam), monoclonal Bcl-x_L (Cell Signaling Technology), polyclonal Sig-1R (previously described in,(Hayashi and Su 2007) polyclonal BiP (BD Bioscience), monoclonal 1,4,5- trisphosphate receptor type 3 (BD Bioscience), and/or monoclonal mitofusin 2 (Abcam) antibodies. After incubation with Alexa-conjugated secondary antibodies, coverslips were mounted on coverglass. Images were analyzed using 3D confocal microscopy using a spinning disk confocal system (Ultraview, PerkinElmer) and inverted microscope (Nikon Eclipse TE2000-E) using a 100× (NA 1.4) oil objective. Colocalization coefficeints, m1 and m2, were used to quantify colocalization (Zinchuk and Grossenbacher-Zinchuk 2001).

Live-cell imaging

CHO-K1 cells transiently transfected with YFP-Bcl-x_L and DsRed-mito were grown on coverslips with poly-D-lysine coating. 24 h after transfection, cells were perfused with RPMI media containing 50 mM HEPES, 10 % FBS and 500 nM thapsigargin (Tg). Images were analyzed using 3D confocal microscopy using a spinning disk confocal system (Ultraview, PerkinElmer) and inverted microscope (Nikon Eclipse TE2000-E) using a 60× (NA 1.4) or 40× (NA 1.3) oil objective. Frames were taken every 30 min for 3 h. Colocalizaztion coefficeints, m1 and m2, were used to quantify colocalization (Zinchuk and Grossenbacher-Zinchuk 2001).

Statistical analysis

Statistical analysis of data provided in this study was determined using analysis of variance (ANOVA) for at least three independent replicates. Values were provided as mean± standard error of mean (SEM), and results with $P < 0.05$ in comparison to an indicated control were considered statistically significant.

Supplementary Material

Refer to Web version on PubMed Central for supplementary material.

Acknowledgments

The authors would like to thank R.Y. Tsien (University of California, San Diego, CA) for generously providing D1ER Ca^{2+} cameleon. We additionally thank J.M. Hardwick (Johns Hopkins University, Baltimore, MD) for providing Bcl-x_L ΔBH4 and Bcl-x_L ΔTM constructs, and Biolog, Inc. for providing the use of its Omnilog microarray system. This work is supported by the NSF and the Intramural Research Program, National Institute of Drug Abuse, NIH, DHHS.

Abbreviations

AUC	Area under the curve
BAPTA	1,2-bis(o-aminophenoxy)ethane-N,N,N’,N’-tetraacetic acid
Bcl-2	B-cell lymphoma-2
Bcl-x_L	B-cell lymphoma-extra large
BiP	Binding immunoglobulin protein
Cyto	Cytosol
DsRed	*Discosoma* sp.red fluorescent protein
ERp75	Endoplasmic reticulum resident protein 75
FRET	Fluorescence energy resonance transfer
Grp75	Glucose regulated protein 75
HcRed	*Heteractis crispa* far-red fluorescent protein
HEPES	4-(2-hydroxyethyl)-1-piperazineethanesulfonic acid
His	Histidine
IP3R	Inositol 1,4,5-trisphophate receptor
IRE1	Inositol-requiring enzyme 1
KHB	Krebs-HEPES Buffer
MAM	Mitochondria-associated ER membrane
Mfn2	Mitofusin 2
Mito	Mitochondria
NAD	Nicotinamide adenine dinucleotide
NADH	Nicotinamide adenine dinucleotide reduced
NP62	Nucleoporin 62
OMM	Outer mitochondria membrane
PERK	RNA-dependent protein kinase-like ER kinase
P1	Whole cell/nuclear
P3	Microsome
RFU	Relative fluorescence units
RLU	Relative fluorescence units

Sig-1R	σ−1 receptor
TCA	Tricarboxylic acid
Tg	Thapsigargin
TM	Transmembrane
Tomm20	Translocase of the outer mitochondrial membrane Tun Tunicamycin
VDAC	Voltage-gated anion channel
YFP	Yellow fluorescent protein

References

Addabbo F et al. (2009) The Krebs cycle and mitochondrial mass are early victims of endothelial dysfunction: proteomic approach. Am J Pathol 1:34–43

Beis I, Newsholme EA (1976) Effects of calcium ions on adenine nucleotide translocase from cardiac muscle. J Mol Cell Cardiol 11: 863–876

Bender E, Kadenbach B (2000) The allosteric ATP-inhibition of cyto-chrome c oxidase activity is reversibly switched on by cAMP-dependent phosphorylation. FEBS Lett 1:130–134

Berridge MJ (2002) The endoplasmic reticulum : a multifunctional signaling organelle, 235–249

Berridge MV, Herst PM, Tan AS (2005) Tetrazolium dyes as tools in cell biology: new insights into their cellular reduction. Biotechnol Annu Rev 05:127–152

Betz C, Stracka D, Prescianotto-baschong C, Frieden M, Demaurex N (2013) Associated endoplasmic reticulum membranes (MAM) regulates mitochondrial physiology

Blackshaw S, Sawa A, Sharp AH, Ross CA, Snyder SH, Khan AA (2000) Type 3 inositol 1,4,5-trisphosphate receptor modulates cell death. FASEB J 10:1375–1379

Boehning D, Patterson RL, Sedaghat L, Glebova NO, Kurosaki T, Snyder SH (2003) Cytochrome c binds to inositol (1,4,5) trisphosphate receptors, amplifying calcium-dependent apoptosis. Nat Cell Biol 12: 1051–1061

Bononi A, Bonora M, Marchi S, Missiroli S, Poletti F, Giorgi C, Pandolfi PP, Pinton P (2013) Identification of PTEN at the ER and MAMs and its regulation of Ca(2+) signaling and apoptosis in a protein phosphatase-dependent manner. Cell Death Differ 12:1631–1643

Bravo R et al. (2011) Increased ER-mitochondrial coupling promotes mitochondrial respiration and bioenergetics during early phases of ER stress. J Cell Sci 14:2511

Brooks C, Cho S, Wang C, Yang T, Dong Z (2011) Fragmented mitochondria are sensitized to Bax insertion and activation during apoptosis, 447–455

Cárdenas C et al. (2010) Essential regulation of cell bioenergetics by constitutive InsP3 receptor Ca2 + transfer to mitochondria. Cell 2: 270–283

Chen ZX, Pervaiz S (2007) Bcl-2 induces pro-oxidant state by engaging mitochondrial respiration in tumor cells. Cell Death Differ 9: 1617–1627

Chen ZX, Pervaiz S (2010) Involvement of cytochrome c oxidase subunits Va and Vb in the regulation of cancer cell metabolism by Bcl-2. Cell Death Differ 3:408–420

Chen R et al. (2004) Bcl-2 functionally interacts with inositol 1,4,5-tris-phosphate receptors to regulate calcium release from the ER in response to inositol 1,4,5-trisphosphate. J Cell Biol 2:193–203

Chen Y et al. (2011) Bcl-xL regulates mitochondrial energetics by stabilizing the inner membrane potential. J Cell Biol 2:263–276

Chiang GG, Sisk WP (2005) Bcl-x(L) mediates increased production of humanized monoclonal antibodies in Chinese hamster ovary cells. Biotechnol Bioeng 7:779–792

Csordás G, Renken C, V'arnai P, Walter L, Weaver D, Buttle KF, Balla T, Mannella CA, Hajn'oczky G (2006) Structural and functional features and significance of the physical linkage between ER and mitochondria. J Cell Biol 7:915–921

Das A (2003) Regulation of the mitochondrial ATP-synthase in health and disease. Mol Genet Metab 2:71–82

Distelhorst CW, Shore GC (2004) Bcl-2 and calcium: controversy beneath the surface. Oncogene 16:2875–2880

Dorai H, Kyung YS, Ellis D, Kinney C, Lin C, Jan D, Moore G, Betenbaugh MJ (2009) Expression of anti-apoptosis genes alters lactate metabolism of Chinese Hamster Ovary cells in culture. Biotechnol Bioeng 3:592–608

Duchen MR (2004) Mitochondria in health and disease: perspectives on a new mitochondrial biology. Mol Asp Med 4:365–451

DuRose JB, Tam AB, Niwa M (2006) Intrinsic capacities of molecular sensors of the unfolded protein response to sense alternate forms of endoplasmic reticulum stress. Mol Biol Cell 7:3095–3107

Eckenrode EF, Yang J, Velmurugan GV, Foskett JK, White C (2010) Apoptosis protection by Mcl-1 and Bcl-2 modulation of inositol 1, 4,5-trisphosphate receptor-dependent Ca2+ signaling. J Biol Chem 18:13678–13684

Eno CO, Eckenrode EF, Olberding KE, Zhao G, White C, Li C (2012) Distinct roles of mitochondria- and ER-localized Bcl-xL in apoptosis resistance and Ca2+ homeostasis. Mol Biol Cell 13:2605–2618

Ezawa I, Ogata E (1979) Ca2 + −induced activation of succinate dehydrogenase and the regulation of mitochondrial oxidative reactions. J Biochem 1:65–74

Gautier C a, Kitada T, Shen J (2008) Loss of PINK1 causes mitochondrial functional defects and increased sensitivity to oxidative stress. Proc Natl Acad Sci U S A 32:11364–11369

Giorgi C et al. (2010) PML regulates apoptosis at endoplasmic reticulum by modulating calcium release. Science 6008:1247–1251

Görlach A, Klappa P, Kietzmann T (2006) The endoplasmic reticulum: folding, calcium homeostasis, signaling, and redox control. Antioxid Redox Signal 9–10:1391–1418

Gülçe Iz S, Çalimlioglu B, Deliloglu Gürhan SI (2012) Using Bcl-xL anti-apoptotic protein for altering target cell apoptosis. EJB 5

Hammerman PS, Fox CJ, Thompson CB (2004) Beginnings of a signal-transduction pathway for bioenergetic control of cell survival. Trends Biochem Sci 11:586–592

Hayashi T, Su T (2007) Sigma-1 receptor chaperones at the ER-mitochondrion interface regulate Ca(2+) signaling and cell survival. Cell 3:596–610

Hayashi T, Su T, Rizzuto R, Hajnoczky G (2009) MAM: more than just a housekeeper. Trends Cell Biol 2:81–88

Hinz JM, Helleday T, Meuth M (2003) Reduced apoptotic response to camptothecin in CHO cells deficient in XRCC3. Carcinogenesis 2: 249–253

Hoseki J, Ushioda R, Nagata K (2010) Mechanism and components of endoplasmic reticulum-associated degradation. J Biochem 1:19–25

Huang H, Hu X, Eno CO, Zhao G, Li C, White C (2013) An interaction between Bcl-xL and the Voltage-dependent Anion Channel (VDAC) promotes mitochondrial Ca2+ uptake. J Biol Chem 27: 19870–19881

Hubbard MJ, McHugh NJ (1996) Mitochondrial ATP synthase F1-beta-subunit is a calcium- binding protein. FEBS Lett 3:323–329

Jahani-Asl A, Cheung ECC, Neuspiel M, MacLaurin JG, Fortin A, Park DS, McBride HM, Slack RS (2007) Mitofusin 2 protects cerebellar granule neurons against injury-induced cell death. J Biol Chem 33: 23788–23798

Jeon MK, Yu DY, Lee GM (2011) Combinatorial engineering of ldh-a and bcl-2 for reducing lactate production and improving cell growth in dihydrofolate reductase-deficient Chinese hamster ovary cells. Appl Microbiol Biotechnol 4:779–790

Jouaville LS, Pinton P, Bastianutto C, Rutter G a, Rizzuto R (1999) Regulation of mitochondrial ATP synthesis by calcium: evidence for a long-term metabolic priming. Proc Natl Acad Sci U S A 24: 13807–13812

Kaufmann T, Schlipf S, Sanz J, Neubert K, Stein R, Borner C (2003) Characterization of the signal that directs Bcl-xL, but not Bcl-2, to the mitochondrial outer membrane. J Cell Biol 1:53

Kirichenko A, Vygodina T, Mkrtchyan HM, Konstantinov A (1998) Specific cation binding site in mammalian cytochrome oxidase. FEBS Lett 3:329–333

Largent BL, Gundlach AL, Snyder SH (1984) Psychotomimetic opiate receptors labeled and visualized with(+)-[3H]3-(3-hydroxyphenyl)-N-(1-propyl)piperidine. Proc Natl Acad Sci U S A 15:4983–4987

Lewis A, Hayashi T, Su TP, Betenbaugh MJ (2014) Bcl-2 family in inter-organelle modulation of calcium signaling; roles in bioenergetics and cell survival. J Bioenerg Biomembr 1:1–15

Li C, Fox CJ, Master SR, Bindokas VP, Chodosh LA, Thompson CB (2002) Bcl-X(L) affects Ca(2+) homeostasis by altering expression of inositol 1,4,5-trisphosphate receptors. Proc Natl Acad Sci U S A 15:9830–9835

Li C, Wang X, Vais H, Thompson CB, Foskett JK, White C (2007) Apoptosis regulation by Bcl-x(L) modulation of mammalian inositol 1,4,5-trisphosphate receptor channel isoform gating. Proc Natl Acad Sci U S A 30:12565–12570

Lu H, Burns D, Garnier P, Wei G, Zhu K, Ying W (2007) P2X7 receptors mediate NADH transport across the plasma membranes of astrocytes. Biochem Biophys Res Commun 4:946–950

Marchi S, Marinello M, Bononi A, Bonora M, Giorgi C, Rimessi A, Pinton P (2012) Selective modulation of subtype III IP(3)R by Akt regulates ER Ca(2)(+) release and apoptosis. Cell Death Dis e304 [PubMed: 22552281]

Mendes CCP, Gomes DA, Thompson M, Souto NC, Goes TS, Goes AM, Rodrigues MA, Gomez MV, Nathanson MH, Leite MF (2005) The type III inositol 1,4,5-trisphosphate receptor preferentially transmits apoptotic Ca2+ signals into mitochondria. J Biol Chem 49: 40892–40900

Meunier J, Hayashi T (2010) Sigma-1 receptors regulate Bcl-2 expression by reactive oxygen species-dependent transcriptional regulation of nuclear factor kappaB. J Pharmacol Exp Ther 2:388–397

Michel AD, Chessell IP, Hibell AD, Simon J, Humphrey PPA (1998) Identi Â® cation and characterization of an endogenous P2X 7 (P2Z) receptor in CHO-K1 cells, 1194–1201

Monaco G et al. (2012) Selective regulation of IP3-receptor-mediated Ca2+ signaling and apoptosis by the BH4 domain of Bcl-2 versus Bcl-Xl. Cell Death Differ 2:295–309

Monserrate J, Chen M, Brachmann C (2012) Drosophila larvae lacking the bcl-2 gene, buffy, are sensitive to nutrient stress, maintain increased basal target of rapamycin (Tor) signaling and exhibit characteristics of altered basal energy metabolism. BMC Biol 1

Mori T, Hayashi T, Hayashi E, Su T (2013) Sigma-1 receptor chaperone at the ER- mitochondrion interface mediates the mitochondrion-ER-nucleus signaling for cellular survival. PLoS One 10, e76941

Ngoh GA, Papanicolaou KN, Walsh K (2012) Loss of mitofusin 2 promotes endoplasmic reticulum stress. J Biol Chem 24:20321–20332

Oakes S a, Scorrano L, Opferman JT, Bassik MC, Nishino M, Pozzan T, Korsmeyer SJ (2005) Proapoptotic BAX and BAK regulate the type 1 inositol trisphosphate receptor and calcium leak from the endoplasmic reticulum. Proc Natl Acad Sci U S A 1:105–110

Palmer AE, Tsien RY (2006) Measuring calcium signaling using genetically targetable fluorescent indicators. Nat Protoc 1:1057–1065 [PubMed: 17406387]

Palmer AE, Jin C, Reed JC, Tsien RY (2004) Bcl-2-mediated alterations in endoplasmic reticulum Ca2+ analyzed with an improved genetically encoded fluorescent sensor. Proc Natl Acad Sci U S A 50: 17404–17409

Pan Z, Damron D, Nieminen AL, Bhat MB, Ma J (2000) Depletion of intracellular Ca2+ by caffeine and ryanodine induces apoptosis of chinese hamster ovary cells transfected with ryanodine receptor. J Biol Chem 26:19978–19984

Pinton P, Ferrari D, Rapizzi E, Francesco DV, Pozzan T, Rizzuto R (2002) A role for calcium in Bcl-2 action? Biochimie 2–3:195–201

Rizzuto R, Diego DS, Raffaello A, Mammucari C (2012) Mitochondria as sensors and regulators of calcium signalling. Nat Rev Mol Cell Biol 9:566–578

Rong Y et al. (2008) Targeting Bcl-2-IP3 receptor interaction to reverse Bcl-2′s inhibition of apoptotic calcium signals. Mol Cell 2:255–265

Rong Y, Humbert DS, Bultynck G, Aromolaran AS, Zhong F, Parys JB, Mignery GA, Roderick HL, Bootman MD, Distelhorst CW (2009) The BH4 domain of Bcl-2 inhibits ER calcium release and

apoptosis by binding the regulatory and coupling domain of the IP3 receptor. Proc Natl Acad Sci U S A 34:14397–14402

Russell JB, Forsberg N (1986) Production of tricarballylic acid by rumen microorganisms and its potential toxicity in ruminant tissue metabolism. Br J Nutr 1:153–162

Scacheri PC et al. (2004) Short interfering RNAs can induce unexpected and divergent changes in the levels of untargeted proteins in mammalian cells. Proc Natl Acad Sci U S A 7:1892–1897

Scorrano L, Oakes SA, Opferman JT, Cheng EH, Sorcinelli MD, Pozzan T, Korsmeyer SJ (2003) BAX and BAK regulation of endoplasmic reticulum Ca2+: a control point for apoptosis. Science (New York, NY) 5616:135–139

Snyder SH, Largent BL (1989) Receptor mechanisms in antipsychotic drug action: focus on sigma receptors. J Neuropsychiatry Clin Neurosci 1:7–15 [PubMed: 2577720]

Su T (1982) Evidence for sigma-opioid receptor: binding of [3H]SKF-10047 to etorphine-inaccessible sites in guinea-pig brain. J Pharmacol Exp Ther 2:284–290

Su Q, Wang S, Gao HQ, Kazemi S, Harding HP, Ron D, Koromilas AE (2008) Modulation of the eukaryotic initiation factor 2 alpha-subunit kinase PERK by tyrosine phosphorylation. J Biol Chem 1:469–475

Szabadkai G, Bianchi K, V'arnai P, De Stefani D, Wieckowski MR, Cavagna D, Nagy AI, Balla T, Rizzuto R (2006) Chaperone-mediated coupling of endoplasmic reticulum and mitochondrial Ca2+ channels. J Cell Biol 6:901–911

Tagami S, Eguchi Y, Kinoshita M, Takeda M, Tsujimoto Y (2000) A novel protein, RTN-XS, interacts with both Bcl-XL and Bcl-2 on endoplasmic reticulum and reduces their anti-apoptotic activity. Oncogene 50:5736–5746

Templeton N, Lewis A, Dorai H, Qian EA, Campbell MP, Smith KD, Betenbaugh MJ, Young JD (2014) The impact of anti-apoptotic gene Bcl-2Δ expression on CHO central metabolism. Metab Eng 25:92–102 [PubMed: 25014175]

Upton J, Austgen K, Nishino M, Coakley KM, Hagen A, Han D, Papa FR, Oakes SA (2008) Caspase-2 cleavage of BID is a critical apoptotic signal downstream of endoplasmic reticulum stress. Mol Cell Biol 12:3943–3951

Vance JE (1990) Phospholipid synthesis in a membrane fraction associated with mitochondria. J Biol Chem 13:7248–7256

Wan B, LaNoue KF, Cheung JY, Scaduto RC (1989) Regulation of citric acid cycle by calcium. J Biol Chem 23:13430–13439

White C, Li C, Yang J, Petrenko NB, Madesh M, Thompson CB, Foskett JK (2005) The endoplasmic reticulum gateway to apoptosis by Bcl-XL modulation of the InsP3R. Nat Cell Biol 10:1021–1028

Xia Z, Liu Y (2001) Reliable and global measurement of fluorescence resonance energy. Biophys J 4:2395–2402

Zannetti A et al. (2008) Gefitinib induction of in vivo detectable signals by Bcl-2/Bcl-xL modulation of inositol trisphosphate receptor type 3. Clin Cancer Res 16:5209–5219

Zhang G, Yan G, Gurtu V, Spencer C, Kain SR (1998) Caspase inhibition prevents staurosporine-induced apoptosis in CHO-K1 cells. Apoptosis 1:27–33

Zheng J, Tsai Y, Kadimcherla P, Zhang R, Shi J, Oyler G a, Boustany NN (2008) The C- terminal transmembrane domain of Bcl-xL mediates changes in mitochondrial morphology. Biophys J 1:286–297

Zinchuk V, Grossenbacher-Zinchuk O (2001) Quantitative colocalization analysis of fluorescence microscopy images In: Anonymous (ed) Current protocols in cell biology. Wiley

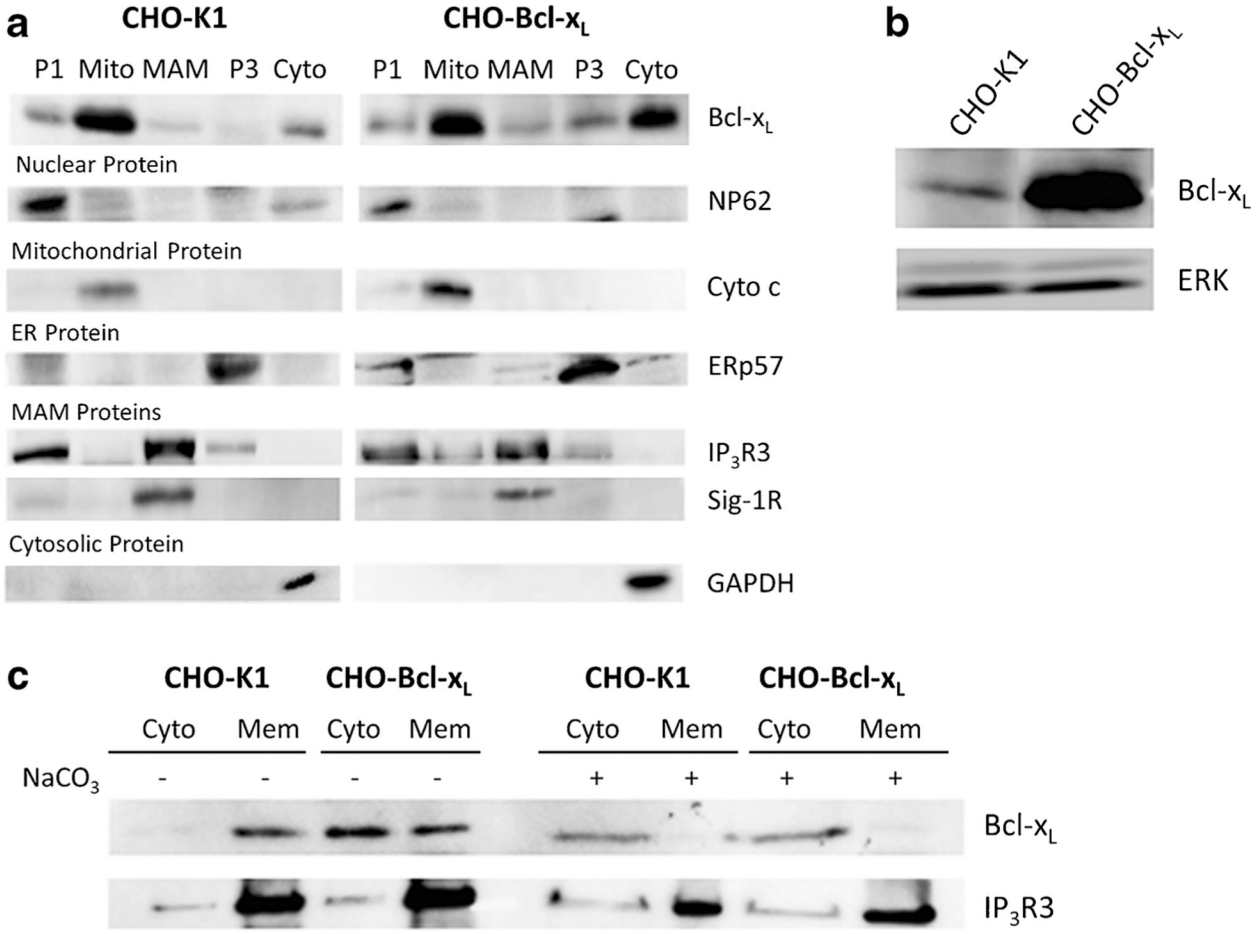

Fig. 1.

Bcl-x_L resides at the MAM. **a** Cell fractionation of CHO-K1 and CHO-Bcl-x_L with markers for known nuclear, mitochondrial, ER, and MAM proteins are used to validate the purity of fractions. P1, whole cell/nuclear; Mito, mitochondria; P3, microsome; Cyto, cytosol. **b** Bcl-x_L expression in CHO-K1 and CHO-Bcl-x_L cells. **c** Bcl-x_L is peripherally attached to cellular membranes, and is thereby released from membrane fractions following alkali treatment (100 mM $NaCO_3$ for 30 min). IP_3R3, a known integral membrane protein, was used for comparison. Mem, crude mitochondrial membrane

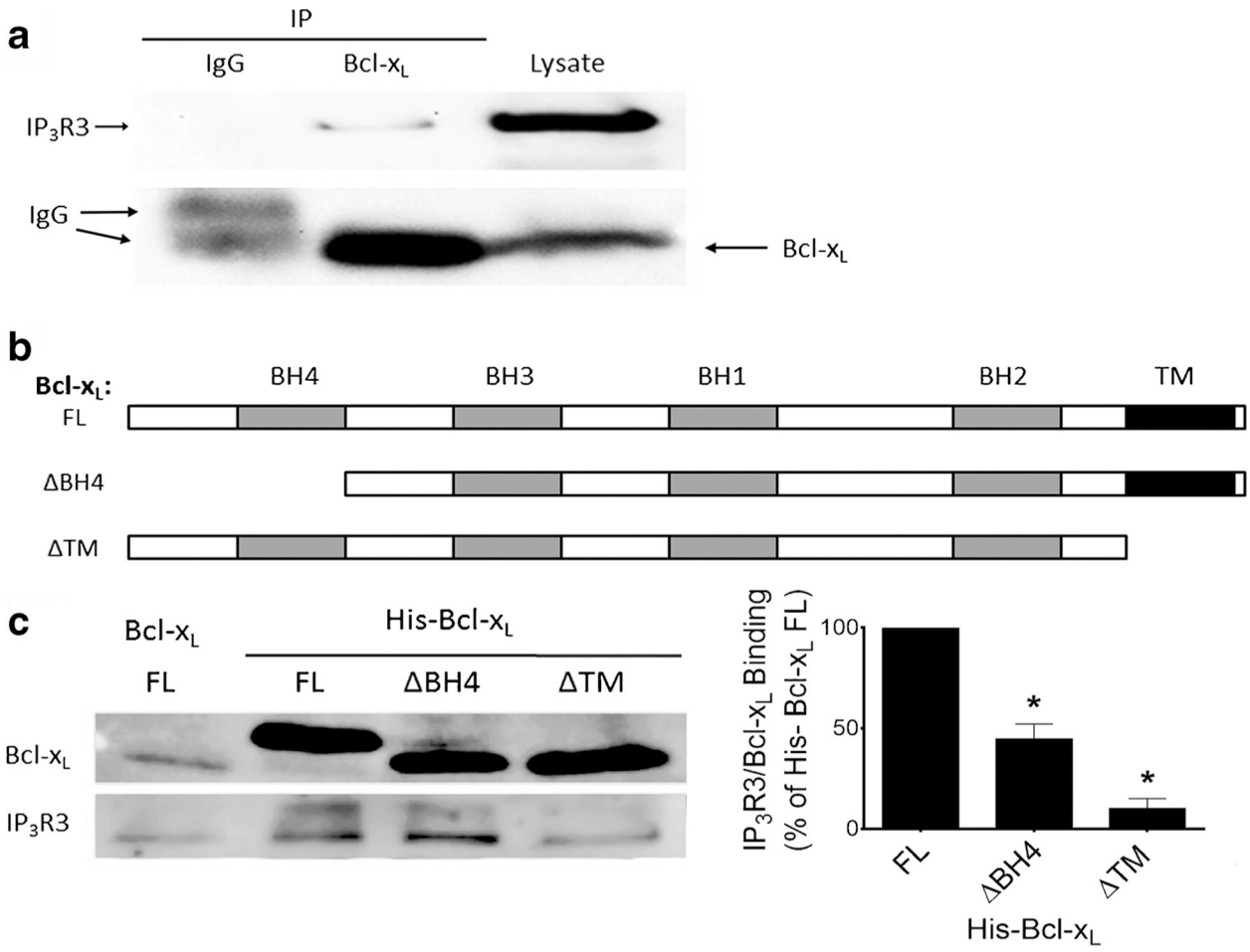

Fig. 2.

Bcl-x_L physically interacts with IP_3R3. **a** IP_3R3 co-precipitates with Bcl-x_L in CHO-Bcl-x_L cells transiently overexpressing IP_3R3. **b** Full-length (FL), BH4-truncated (ΔBH4), and TM domain-truncated (ΔTM) Bcl-x_L constructs. **c** A comparison of IP_3R3/Bcl-x_L binding by nickel pull-down of Bcl-x_L in CHO-K1 cells transiently overexpressing FL, ΔBH4, or ΔTM his-tagged Bcl-x_L. Endogenous IP_3R3 interaction with FL His-Bcl-x_L is taken as one hundred percent. Data represented as mean ± SEM ($n = 4$). *$P < 0.05$ versus full-length Bcl-x_L

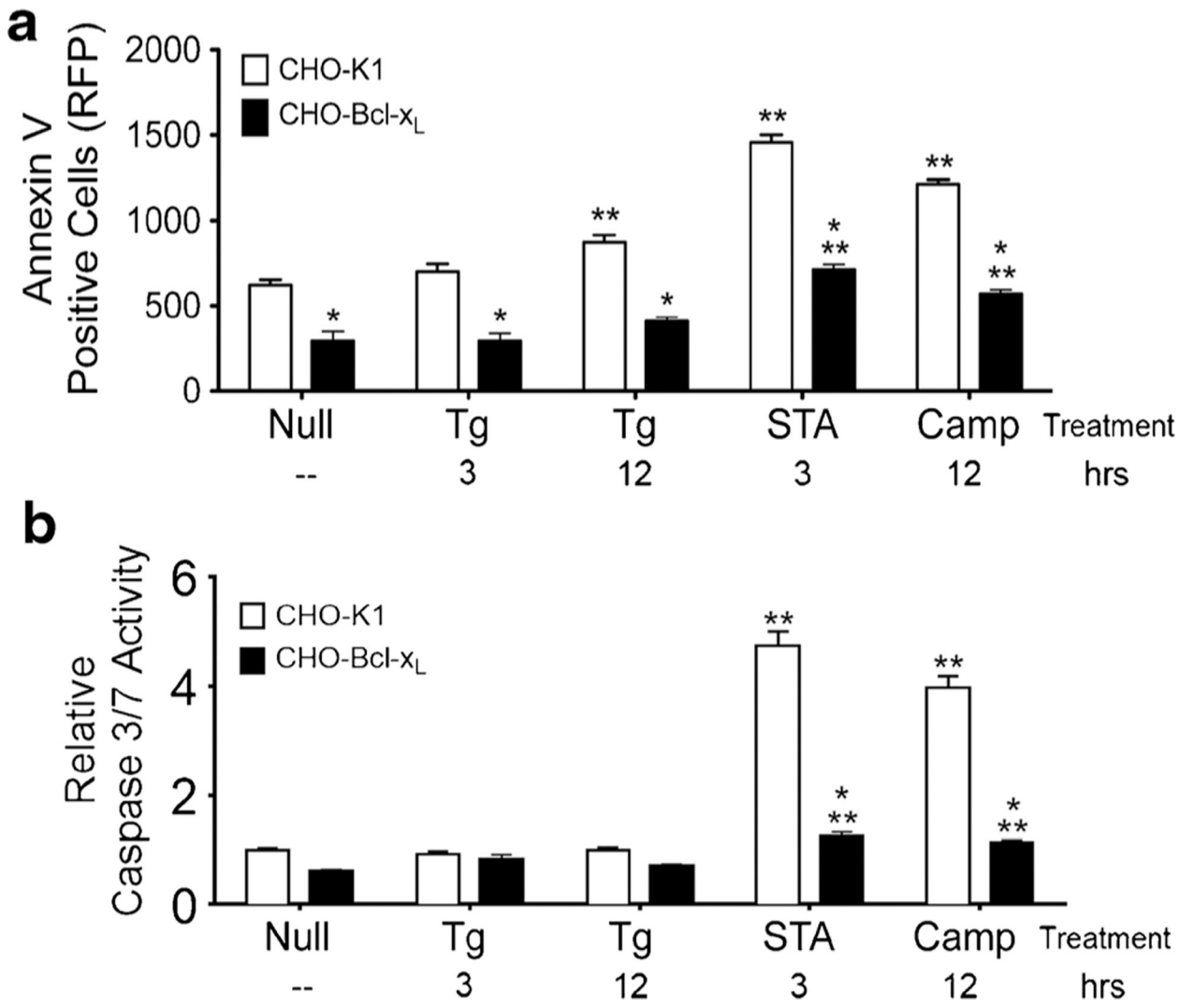

Fig. 3.

Limited thapsigargin treatment does not induce apoptosis. **a** In comparison to known apoptosis-inducing compounds, staurosporine (3 uM STA, 4 h) or camptothecin (50 uM Camp, overnight), there is not a significant increase in apoptosis due to prolonged treatment with Tg as indicated by Annexin V positive cells ($n = 3$). **b** There is not a significant activation of caspase 3/7 activities in comparison to known apoptosis-inducing compounds (STA or Camp) following prolonged Tg treatment ($n = 3$). 500 nM Tg treatment was used for all experiments. *$P < 0.05$ versus control at identical time point. **$P < 0.05$ versus non-treated control of the same cell line

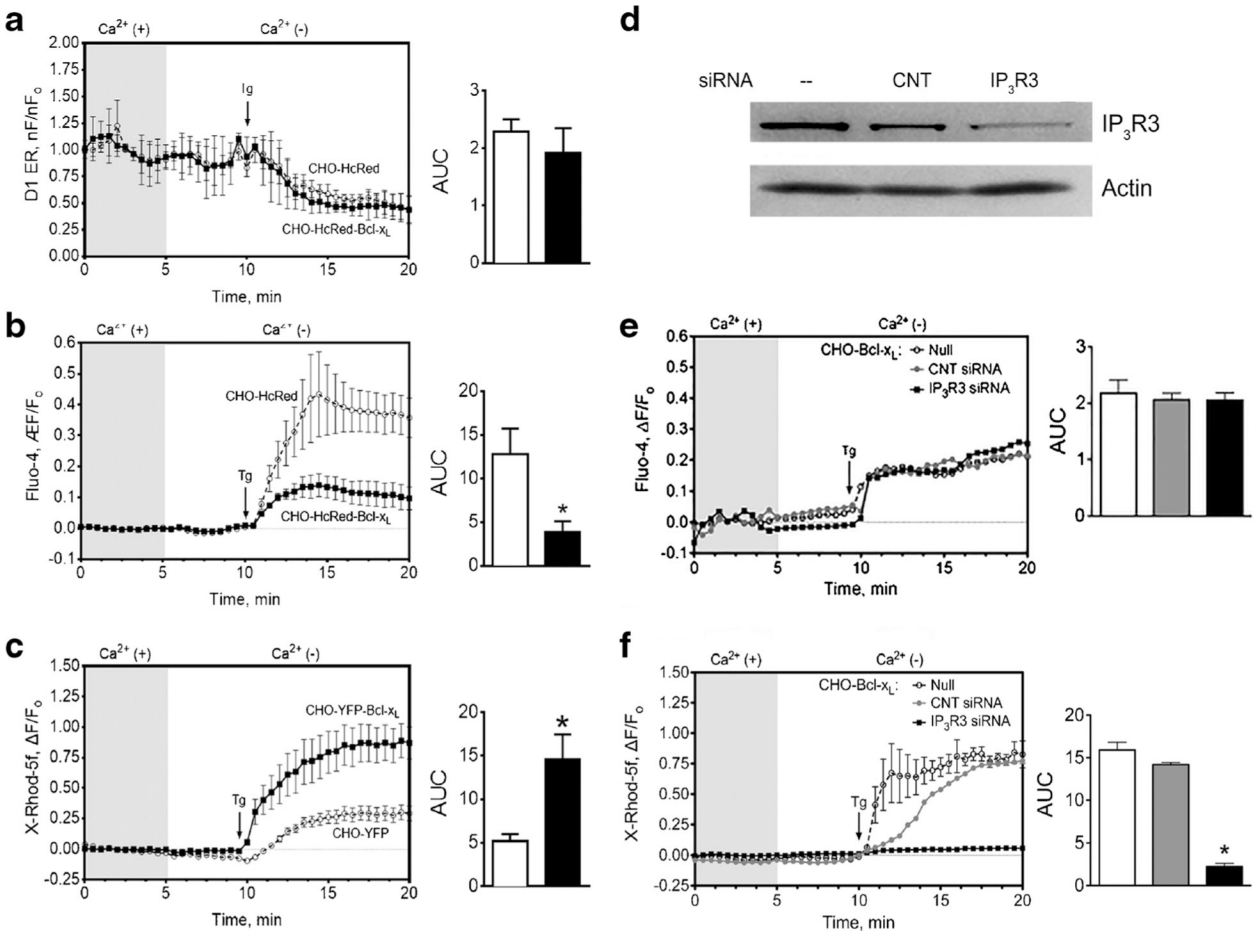

Fig. 4.

MAM-associated Bcl-x_L modulates IP_3R-mediated Ca^{2+} signaling. Ca^{2+} signaling was compared in co-cultured control (CHOYFP or CHO-HcRed) and Bcl-x_L overexpressing cells (CHO-YFP-Bclx_L or CHO-HcRed-Bcl-x_L) in response to 500 nM Tg treatment. During experimentation, cells were perfused in Ca^{2+}(+) Krebs-HEPES Buffer (KHB) for 5 min, followed by perfusion in Ca^{2+}(−) KHB. **a** Net FRET (nF) measurement, FRET measurement corrected for background, of ER Ca^{2+} using D1ER Ca^{2+} cameleon shows no significant difference in ER Ca^{2+} depletion in Bcl-x_L overexpressing cells compared to control ($n = 3$). **b** ER to cytosol Ca^{2+} influx was measured using Fluo-4 AM Ca^{2+} dye ($n = 5$). A smaller increase in cytosolic Ca^{2+} influx was observed in Bclx_L overexpressing cells. **c** ER to mitochondria Ca^{2+} influx was measured using X-Rhod-5f AM Ca^{2+} dye ($n = 5$). A larger increase in mitochondrial Ca^{2+} influx was observed in Bcl-x_L overexpressing cells relative to control cells. **d** CHO-Bcl-x_L cells were transfected with non-active control siRNA (CNT siRNA) or siRNA targeting IP_3R3. Ca^{2+} signaling was compared in co-cultured null (non-siRNA treated) cells and siRNA treated (CNT or IP_3R3) cells. **e** Knocking down IP_3R3 does not affect ER to cytosolic Ca^{2+} transfer, but **f** significantly diminishes ER to mitochondrial Ca^{2+} transfer in CHO-Bcl-x_L cells ($n = 3$). All data represented as mean ± SEM. $^*P < 0.05$ versus control. AUC, or area under the curve, is provided as a comparison

of calcium transients between cell lines, as it takes into account differences in the fluorescence baseline fluorescence between cells

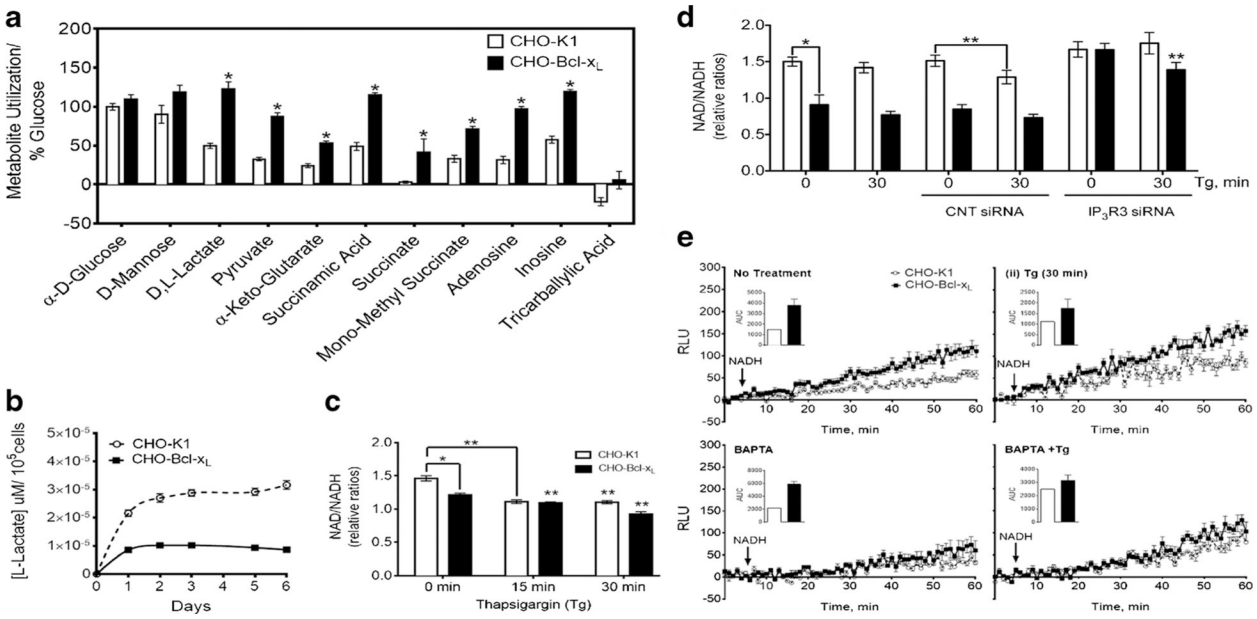

Fig. 5.

Bcl-x expression facilitates Ca^{2+}− dependent TCA cycle activity. **a** Metabolic consumption rates of key metabolites contained on PM-M1 Phenotype MicroArray plates were evaluated in CHO-K1 and CHO-Bcl-x_L cells ($n = 3$). Wells containing α-D-glucose serve as a positive control, while tricarballylic acid, an inhibitor of aconitase, functions as a negative control. All rates normalized to the slope of glucose consumption. **b** Lactate accumulation was reduced in Bcl-x_L overexpressing cells compared to controls ($n = 3$). **c** Relative NAD/NADH ratios were reduced in Bcl-x_L overexpressing in comparison to control cells. Incubating cells with Tg for 15 or 30 min causes a further reduction in NAD/NADH ($n = 3$). **d** Higher NAD/NADH (relative ratios) are observed when IP_3R3 is knocked down using siRNA compared to null cells, while control (CNT) NADH ratios/NADH ratios ($n = 3$). (Di) Electron transport chain (ETC.) oxidase activity is higher in Bcl-x_L overexpressing cells compared to controls in non-treated cells ($n = 6$). Pre-incubation with (Dii) Tg, (Diii) BAPTA-AM, a Ca^{2+} chelater, (Div) or a combination of both also alters NADH oxidation ($n = 3$). ROC, rate of change. All data is represented as mean ± SEM. $^*P < 0.05$ versus control at identical time point. $^{**}P < 0.05$ versus non-treated, or initial time point, control of the same cell line

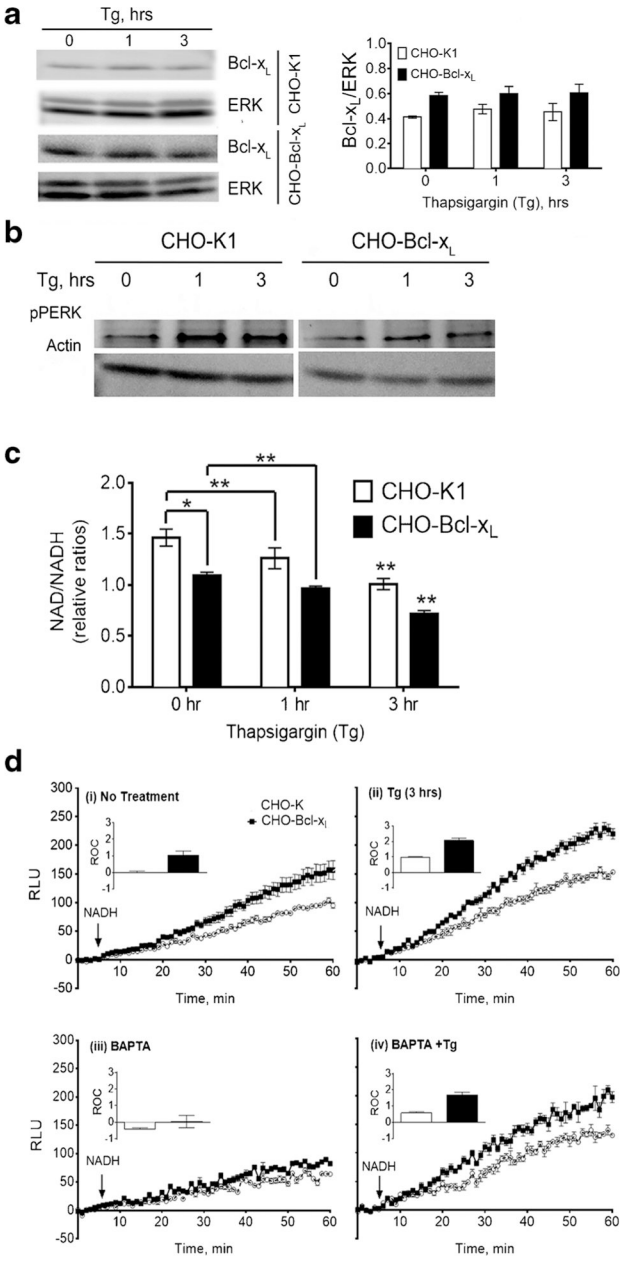

Fig. 6.

Bcl-x_L expression enhances TCA cycle activity during ER stress conditions. **a** Bcl- x_L protein levels are not significantly altered in control and Bcl-x_L overexpressing cells after 1 and 3 h treatment with Tg ($n = 3$). **b** Activation of ER stress, as indicated by the upregulation of phosphorylated PERK (pPERK), is detected in both endogenous and Bcl-x_L overexpressing cell lines, but is most notable in CHO-K1 cells. **c** Substantial increases in NADH production, as indicated by reduced NAD/NADH (relative ratios), are observed following 1 or 3 h Tg insult, particularly in Bcl-$x_L$overexpressing cells. (Di) Electron transport chain (ETC.) oxidase activity in non-treated CHO-K1 and CHO-Bcl-x_L cells. (Dii) In comparison, ETC.oxidase activity is significantly enhanced when cells are incubated with Tg for 3 h. (Diii-iv) This effect is hindered by pre-treating cells with BAPTAAM. Overall,

ETC. oxidase activity remains higher in Bcl-x_L expressing cells. ROC, rate of change. 500 nM Tg treatment was used for all experiments. All data represented as mean ± SEM for three independent experiments. *$P < 0.05$ versus control at identical time point. **$P < 0.05$ versus non-treated control of the same cell line

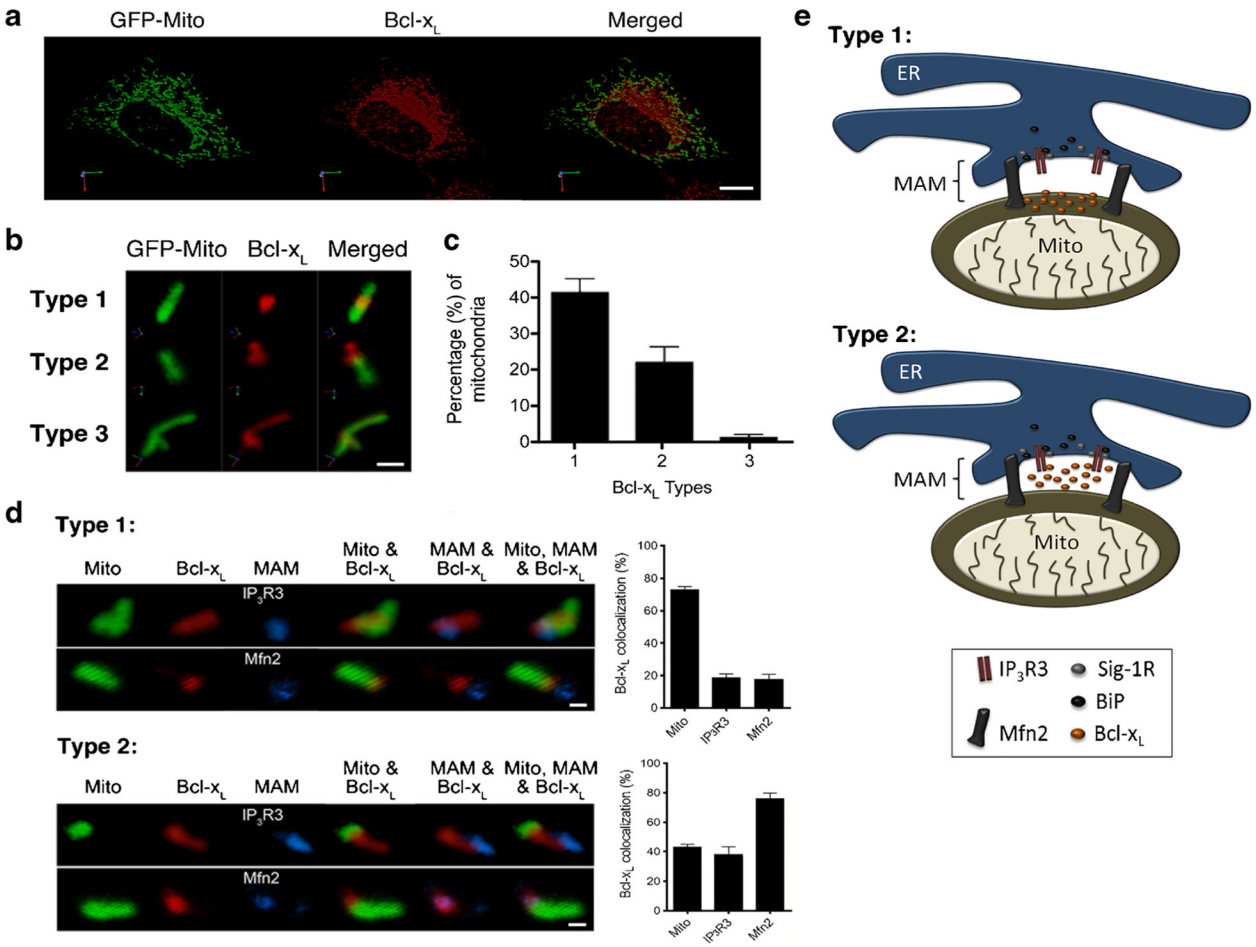

Fig. 7.

Three distinct patterns of Bcl-x_L in relation to mitochondria. **a** Immunostaining of CHO-Bcl-x_L (*red*) transiently transfected with GFP-mito (*green*). Areas in which Bcl-x_L and mitochondria co-localize are observed in *yellow*. Scale bar = 10 μm. **b** Bcl-x_L was categories into three distribution patterns based on its relation to mitochondria—Type 1: clustered residing on mitochondria (≥50 % Bcl-x_L colocalization), Type 2: clustered adjacent to mitochondria (<50 % Bcl-xL colocalization), or Type 3: evenly distributed on mitochondria. **c** Mitochondria with exclusively Type 1 Bcl-x_L were the most prominent, followed by mitochondria exhibiting Bcl-x_L exclusively in a Type 2 pattern. Only a small percentage of mitochondria were observed exclusively with Type 3 Bcl-x_L. Data represented as mean ± SEM (n = 300). Scale bar = 2 μm. **d** Immunostaining and co-localization of Type 1 and Type 2 Bcl-x_L (*red*) with GFP-mito (*green*) and MAM marker proteins (*blue*)—IP_3R3 and Mfn2 (a MAM-mitochondria tethering protein). Data represented as mean ± SEM (n = 6). Scale bar = 2 μm. **e** Schematic representation of mitochondria with Type 1 and Type 2 Bcl-x_L and its association with the MAM are depicted

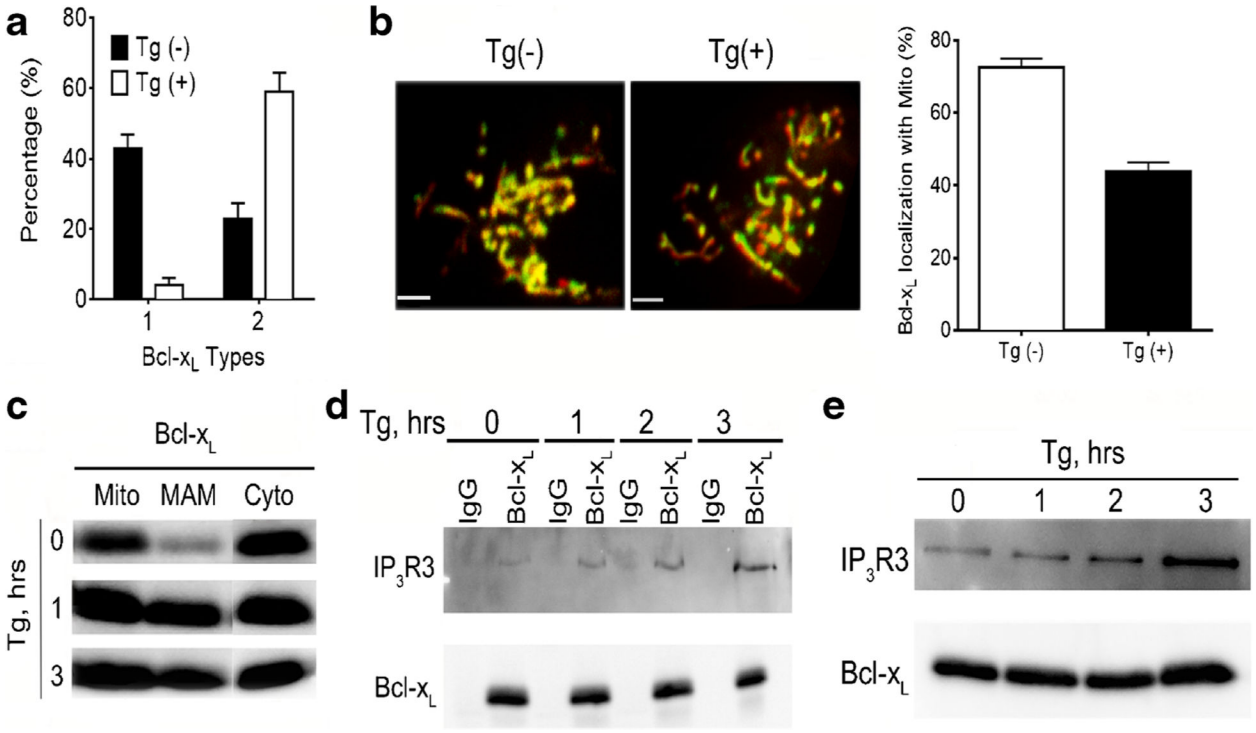

Fig. 8.

Bcl-x_L translocates to MAM following thapsigargin treatment. **a** Tg treatment (3 h) resulted in an increase in the number of Type 2 Bcl-x_L, and a corresponding decrease in Type 1 Bcl-x_L in immunostained CHOBcl-x_L cells ($n = 300$). **b** Decreased Bcl-x_L co-localization with mitochondria was observed during live-cell imaging of CHO-YFP-Bclx_L cells transiently transfected with DsRed-mito and incubated with Tg over a 3 h time-span ($n = 3$). Bcl-x_L is depicted in *green* and mitochondria is depicted in *red*, while overlapping is depicted in *yellow*. Bcl-x_L co-localization with mitochondria decreases after Tg treatment, and more distinct *green* and *red* fluorescence is observed. **c** Cell fractionation studies showed decreases in overexpressed Bcl-x_L at mitochondria-enriched fractions, and corresponding increases at MAM-enriched fractions after prolonged Tg treatment (1 and 3 h). Additionally, Tg treatment increased interaction of Bcl-x_L with IP_3R3 over a 3 h time-span as indicated by **d** immunoprecipitation and e nickel pull-down. 500 nM Tg treatment was used for all experiments. Data is represented as mean ± SEM ($n = 3$). *$P < 0.05$ versus non-treated control